

Synthesis and Characterization of Nanocrystalline Barium Strontium Titanate Powder by Mechano-Chemical Method

V.G.Ugalmogale¹, R.B.Ahirrao^{2*}

¹Department of Physics, Karm. A.M. Patil Arts, Commerce and Kai. Annasaheb N.K. Patil Science College, Pimpalner, KBC North Maharashtra University Jalgaon, Dhule-424304, Maharashtra, India.

²Material Science Laboratory, P.G. department of Physics, Pratap College, KBC North Maharashtra University Jalgaon Amalner- 425401, Maharashtra, India.

Corresponding Author: R.B.Ahirrao

Abstract: The nanocrystalline Barium Strontium Titanate (BST) powders were synthesized by mechanochemical method using barium carbonate ($BaCO_3$), titanium dioxide (TiO_2) and strontium carbonate ($SrCO_3$) as the precursors. Conventional ball-milling also preferred to get average particle size. The powder was sintered at $600^\circ C$, $750^\circ C$ and $800^\circ C$. X-ray Diffraction (XRD) technique was used to know structural properties of BST powder and EDAX is used for quantitative elemental analysis. The decomposition and crystalline behavior of BST were examined by Thermogravimetric and Differential Thermal Analysis (TG-DTA). Scanning Electron Microscopy (SEM) investigation was performed to examine grain size and microstructural properties of BST powder. The UV-Vis spectrum used for band gap calculation. Raman spectroscopy was used for the confirm the phase. The samples were characterized by infrared spectroscopy method (FT-IR). The results showed that the obtained crystallite sizes were 33 and 37 nm for BST powder sintered at 750 and $800^\circ C$, respectively.

Keywords: Mechanochemical synthesis, sintering, BST nanopowder, Particle size, XRD

Date of Submission: 18-03-2019

Date of acceptance: 02-04-2019

I. Introduction

Perovskite-oxides have been extensively studied due to their excellence in electrical [1] and optical properties [2-3]. Recently, perovskite-oxides have attracted great interest in their use as nanocatalysts in the photocatalytic decolorization of methylene blue applications such as $BaTiO_3$ [4], $SrTiO_3$ [5], $CaTiO_3$ [6-7], and $Ba_{1-x}Sr_xTiO_3$ (BST) [8].

Since the report that ferroelectric materials can be used to fabricate large scale integrated circuit (VLSI) memory, Post-Gbit dynamic random access memory (DRAM) capacitors prepared via ferroelectric materials have attracted considerable attentions in recent years. Barium strontium titanate (BST) is an attractive capacitor material for dynamic random access memories and infrared detectors due to its chemical stability, excellent structure and dielectric properties compared to other ferroelectric materials such as $BaTiO_3$, $PbTiO_3$, etc. [9-14]. $BaTiO_3$ and $SrTiO_3$ are representative ABO₃ model perovskite materials and BST is also a solid solution system between $BaTiO_3$ and $SrTiO_3$, i.e., $Ba_{1-x}Sr_xTiO_3$ simultaneously has the advantages of the high dielectric constant of $BaTiO_3$ and the structural stability of $SrTiO_3$. At room temperature, it is known that the solid solution system is in a ferroelectric phase when Ba content 1-x is in a range from 0-0.7 [15-16]. Furthermore, the electrical properties of BST such as dielectric constant, dielectric loss, depend upon the composition, dopant, microstructure, etc. and the electrical properties and kinetic behaviours of undoped and doped BST have been fully investigated [17-18]. However, the characterizations of doped BST, especially manganese, which has an influence on the grain boundary resistance [19-21], have been insufficiently investigated. It is concluded that dopant can significantly modify the dielectrical and electrical properties of ferroelectric materials such as barium strontium titanate (BST), lead zirconate titanate (PZT), etc.

Barium strontium titanate (BST) or $BaTiO_3$ has been prepared by a variety of different techniques, for example Xu *et al.* [22] prepared nanosized $BaTiO_3$ powders by hydrothermal method; but among them, the solid state reaction method is the traditional method for preparing $BaTiO_3$ powders by mixing the starting materials, usually titanium dioxide and barium carbonate and calcinations them at an elevated temperature around $1200^\circ C$. However, the solid-state reaction method tends to result in a significant amount of agglomeration, poor chemical homogeneity and undesirable secondary phase such as $BaTi_2O_5$.

It is known that the mechanochemical synthesis relates to non-conventional methods of green chemistry since it allows decreasing the pollution in the environment [23-26]. The main purpose of present work

is to prepare the BST powder through mechanochemical method and investigate the structural, optical properties of the so prepared powder.

Mechanochemical reaction is a process that a strong mechanical force proceeds materials destruction and causes a formation of a different structure. Mechanochemical method has been widely used in synthesis of advanced materials, covered almost all aspects of material science [27-29]. Mechanochemical process is a simple, environmental, low-cost technology. Interests in this field tend to rise continuously, and the number of related papers increases annually [30-32].

II. Materials and Methods

2.1. Synthesis of BST powder

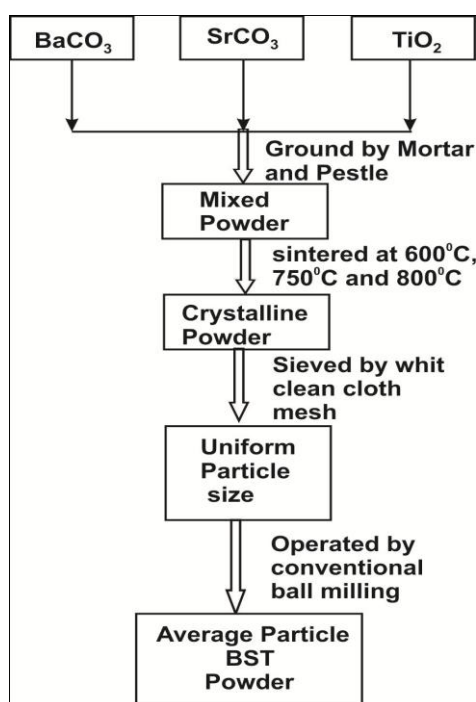


Fig. 1. Flow chart of synthesis of Nanostructured BST powder preparation

Barium carbonate (BaCO_3), titanium dioxide (TiO_2) and strontium carbonate (SrCO_3) were mixed by solid state mixed oxide route. This powder was mixed by using mortar and calcined at 200°C for 1 h and 30 min in order to decarbonate. BST crystalline powder was sieved with cleaned white clothes mesh sieve to get uniform grain/particle size. This powder was operated by ball mill to reduce particle size. As a result, the homogeneous and moisture-less crystalline BST powder was formed at a given temperature. The flow diagram of preparation of BST powder was indicated in Fig.1. The BST powder then sintered at 600°C , 750°C and 800°C .

III. Result And Discussion

3.1. Thermal study of BST powders

3.1.1. TGA-DTA study

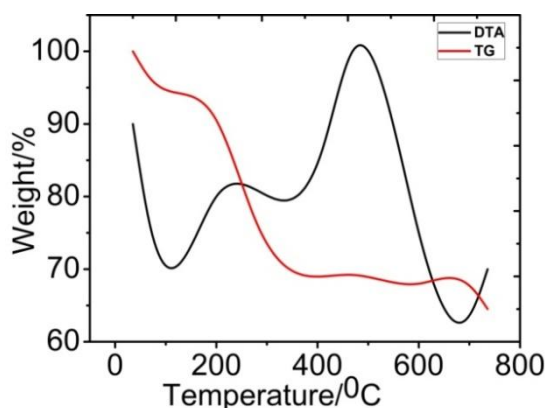


Fig. 2. TGA–DTA curves of the nanocrystalline BST powder.

The TG-DTA analysis was carried out on WCT-2A apparatus at a heating rate of 10 °C/min under a dry air atmosphere, heated up to 900 °C and the result was shown in Fig. 1. Thermal analysis gives information about changes in material properties as function of temperature. The TGA only measures changes caused by mass loss, DTA also register changes in material where no mass loss occur, From the TG–DTA curves, the heat-treatment process could be divided into three steps. First 2.27% weight loss below 300°C; the second weight loss at the temperature between 300°C and 500°C which is 4.3%. They are supposed to be the results of both endotherm and exotherm which are caused by further weight loss of the combustion and exothermal reaction between different components. When the temperature is above 450°C, there is a 5.2% loss of weight.

3.2. Structural properties

3.2.1. XRD Analysis of BST nanopowder

From the XRD spectrum it is observed that the peaks corresponding to the powder sintered at 600°C are faint however powder sintered at 750 and 800°C are observed to be prominent therefore it is concluded that the powder (particles) are not fully crystalline. It can be seen that at 600°C, a weak line occurs at 24.2 which corresponds to the residual carbonates phase such as BaCO₃, SrCO₃ and (Ba, Sr) CO₃ [33]. At temperatures these peaks disappear and a pure BST phase is identified at 750°C and 800°C. This indicates that as the temperature increases, the residual carbonates decompose. This can be confirmed by FT-IR analyses of BST powders sintered at 750°C and 800°C. The phase confirms the Barium Strontium Titanate’s perovskite phase which is in good agreement with literature results.

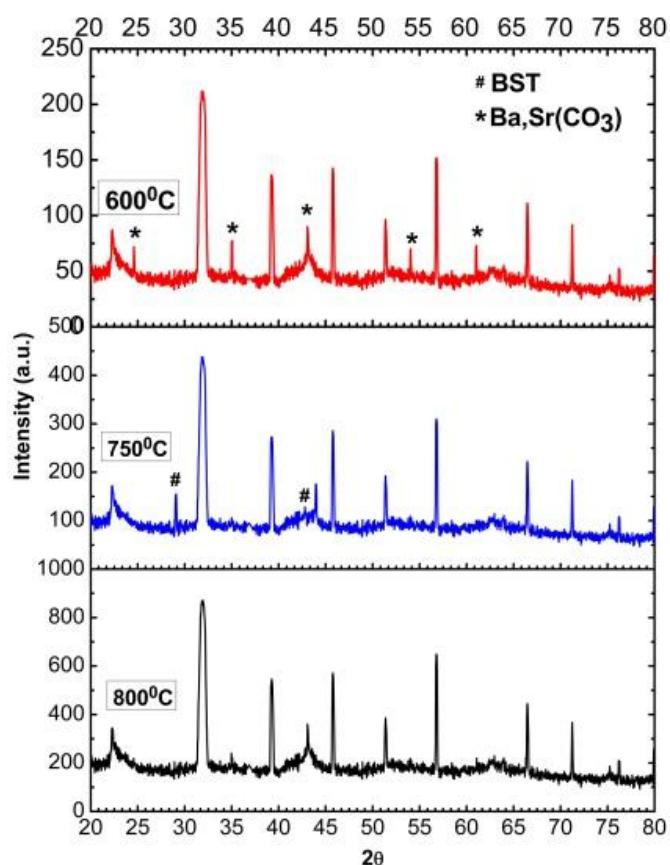


Fig. 3.XRD patterns of the BST powders sintered at 600, 750 and 800°C.

The peaks associated with the barium carbonate secondary phases are marked with asterisks. The crystallite size of the synthesized BST powder was calculated using Scherrer’s formula:

$$D = \frac{0.9\lambda}{\beta \cos \theta}$$

Where D is the average grain size, $\lambda = 1.541\text{Å}$ X-ray wavelength, and β is the width of the diffraction peak at half maximum for the diffraction angle 2θ .

Table: 1. Details of the calculated X-ray spectrum for BST powder sintered at 750 °C.

hkl	2θ (deg)	d _{hkl} [Å]	FFWHM (deg)	Particle size (nm)
100	22.265	3.9893	0.1993	40.61
110	31.827	2.8092	0.2709	34.08
111	39.268	2.2867	0.3145	27.40
200	75.241	1.9826	Average	33.31
310	75.892	1.2523	---	---
311	75.892	1.1979	---	---
222	84.605	1.1424	---	---

3.1.2. SEM study of BST nanopowder

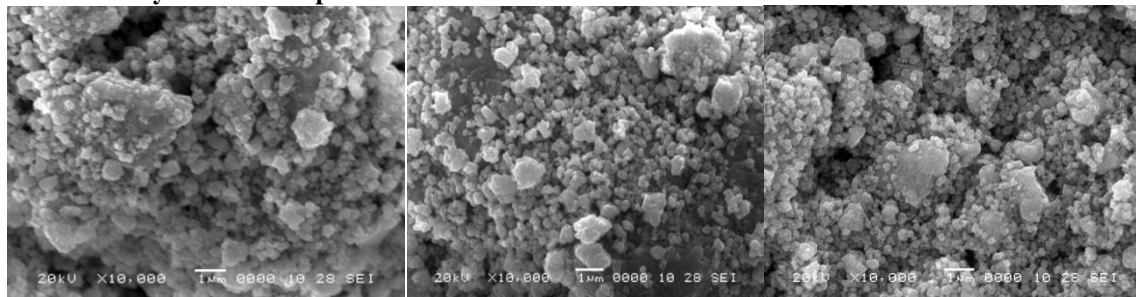


Fig. 4. SEM images of (a) 600⁰C, (b) 750⁰C and (c) 800⁰C sintered BST powder.

Figure 3. (a),(b) and (c) shows the SEM morphology of the synthesized nanocrystalline powders sintered at (a) 600⁰C, (b) 750⁰C and (c) 800⁰C using mechanochemical method. The powders obtained contain a large portion of agglomerates with a small particulate size and some of shows multilayer deposition. Since the agglomeration was sufficiently large and soft. It could be clearly observed that the agglomerates are actually formed very small particles in nanometric range size. It could be clearly observed that the agglomerates are actually formed very small particles in nanometric range size. Although the agglomerates are of irregular size the fine nanometric particles are mostly below 100 nm in size.

3.1.3. Quantitative elemental analysis

Table: 2. Stoichiometric analysis of BST powder; Table: 3. Particle elemental analysis of BST powder

Element	Atomic mass	No of Atoms	Mass %
Ba	137.327	1	42.80
Sr	87.62	1	27.31
Ti	47.867	1	14.91
O	15.999	3	4.98

Element	Mass %	Atomic%
Ba	45.22	55.41
Sr	39.13	15.00
Ti	15.62	21.38
o	01.13	09.31

The quantitative elemental composition of BST powder and mass % of BST, were analyzed using an energy dispersive spectrometer are represented in Table 2 &3. The table shows that the BST powder is observed to be oxygen rich. Excess or deficiency of the constituent material particles leads the semiconducting nature of the material.

3.2. Optical properties

3.2.1. UV-Visible spectrum

It is known that in the absorption process, a photon of known energy excites an electron from lower to a higher energy state, corresponding to an absorption edge. In crystalline materials, the fundamental edge is directly related to the conduction and valence band; that is, direct and indirect band gaps. The diffuse reflectance spectrum is recorded in the range of 300-800 nm for finding optical band gap energy of powder samples. It is observed that the curves for this sample shifted to higher wavelengths, indicating a increase in the optical gap.

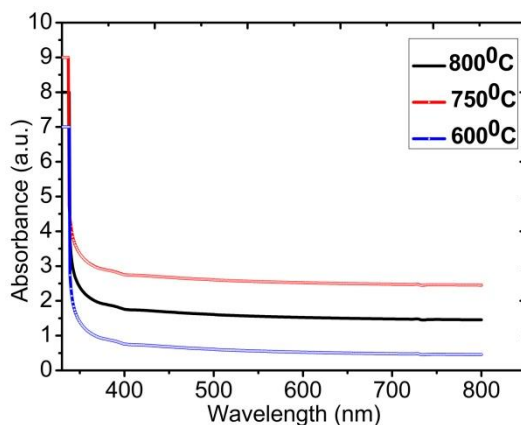


Fig.5. Observed absorption spectra of BST powder sintered at 600°C, 750°C and 800°C.

3.2.2. Tauc's Plot (Band gap energy)

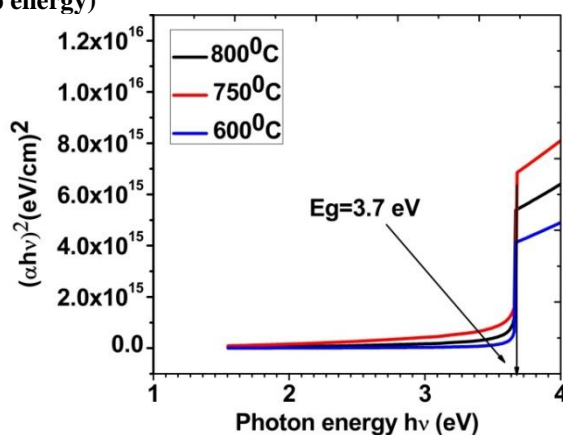


Fig. 6. Variation of $(\alpha hv)^2$ versus photon energy (hv).

The optical band gap value can be determined from the Tauc's relation [34]

$$\alpha = \frac{(hv - E_g)^n}{hv}$$

Where- E_g the optical band gap and n is the index representing the transition order. Here band gap energies of indirect transition should be considered [35] with regard to indirect transition, Thus, the E_g of the indirect transition can be derived from the dependence of the $(\alpha hv)^2$ on the photon energy hv . In energy regions higher than the absorption edge, $(\alpha hv)^2$ against the hv showed a straight line in each particle size, which insures the linear relation between $(\alpha hv)^2$ and hv . The above equation demonstrates that an extrapolation of the tangential line from high photon energy intersects $(\alpha hv)^2 = 0$ at $hv = E_g$, which gives the band gaps of BST nano particles. In the present estimation, the tangential lines in the energy region from 3.7 eV were extrapolated.

3.2.3. Raman spectrum

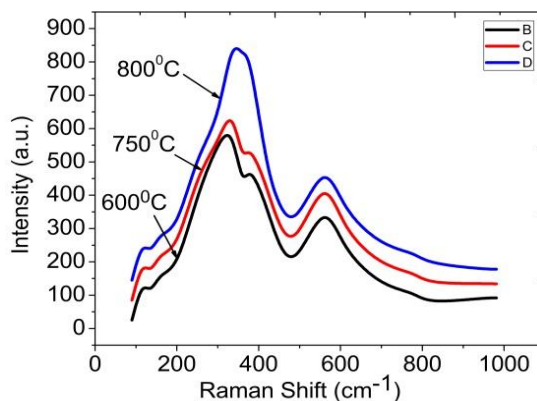


Fig.7. Raman spectra of the powder BST powder sintered at 600°C, 750°C and 800°C.

Raman spectra of the BST powder sintered at various temperatures are shown in figure 4 between 200 and 300 cm^{-1} . It is observed from figure that are two modes boated around 218 and 250 cm^{-1} . The increase in sintering temperature causes gradual decrease in intensity [36]. The increase in lattice parameter indicates a trend towards the tetragonal phase. The mode around 305 cm^{-1} may be due to cubic phase. Besides, we have observed the presence of two bands at around 117 and 804 cm^{-1} , which have not been reported in the literature; their presence may be related to the secondary phase BaSrCO_3 , in accordance with XRD observation.

3.2.4. FT-IR analysis

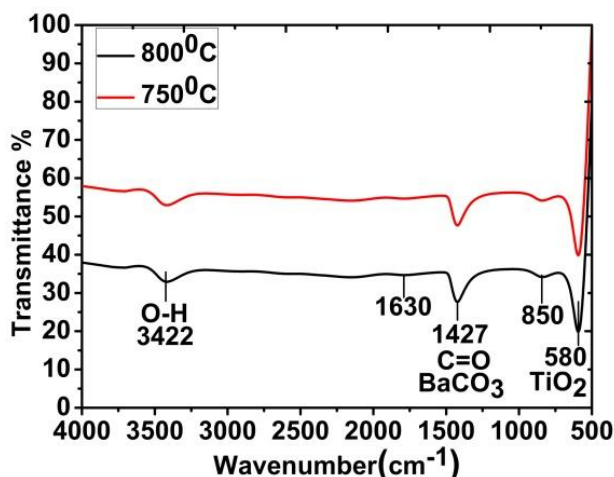


Fig.8. Shows the FT-IR spectra of BST powder sintered at 600 $^{\circ}\text{C}$, 750 $^{\circ}\text{C}$ and 800 $^{\circ}\text{C}$.

The broad band at 3422 cm^{-1} is related to O–H stretching modes of absorbed water by KBr pellets that were used for FT-IR spectroscopy [37]. The peaks corresponding to barium carbonate are evident at 1630, 1427, 850 and 580 cm^{-1} [38]. The absorption band at 1427 cm^{-1} can be interpreted as C=O vibration due to extremely small unavoidable traces of carbonate. It can be seen that as the temperature increases, the amount of carbonates formed decreases. Hence, the result shows that the nanopowders obtained at 800 $^{\circ}\text{C}$ are more pure than those obtained at 750 $^{\circ}\text{C}$. Furthermore, the absorption band at 611 cm^{-1} is assigned to specific vibrations of Ti–O bonds [39]. As can be seen, the value of absorption at 611 cm^{-1} (Ti–O bonds) for BST powder sintered at 800 $^{\circ}\text{C}$ is higher than that of BST powder calcined at 750 $^{\circ}\text{C}$. This may be due to the purity, crystallinity and particle size of BST powder sintered at 800 $^{\circ}\text{C}$.

IV. Conclusion

Nanocrystalline BST powder has been successfully synthesized by a mechanochemical technique. The XRD patterns confirmed the cubic structure of the so prepared samples. XRD and FT-IR analyses revealed that pure phase BST can be obtained above 750 $^{\circ}\text{C}$. The average of particle size calculated from the XRD pattern was 33 and 37 nm for sintering temperatures 750 $^{\circ}\text{C}$ and 800 $^{\circ}\text{C}$, respectively. FESEM investigation showed that the nanoparticles obtained at 800 $^{\circ}\text{C}$ were more agglomerated and larger in size than those obtained at 750 $^{\circ}\text{C}$. The mechanochemical method can be used to deposit nano-thin films of BST powder for applications in sensors.

Acknowledgement

Authors are thankful to department of Physics and Institute of sophisticated instruments; university of Pune for characterizations, Authors are also thankful to Principal and in-charge department of sophisticated instruments; Pratap College Amalner to allow the laboratory facility.

Reference

- [1]. B. Hou, Y. Xu, D. Wu, and Y. Sun, "Preparation and characterization of single-crystalline barium strontium titanate nanocubes via solvothermal method," *Powder Technology*, vol. 170, no. 1, pp. 26–30, 2006.
- [2]. F.M. Pontes, E. Longo, E. R. Leite et al., "Photoluminescence at room temperature in amorphous SrTiO_3 thin films obtained by chemical solution deposition," *Materials Chemistry and Physics*, vol. 77, no. 2, pp. 598–602, 2003.
- [3]. F. M. Pontes, C. D. Pinheiro, E. Longo et al., "Theoretical and experimental study on the photoluminescence in BaTiO_3 amorphous thin films prepared by the chemical route," *Journal of Luminescence*, vol. 104, no. 3, pp. 175–185, 2003.
- [4]. S. Otsuka-Yao-Matsuo, T. Omata, S. Ueno, and M. Kita, "Photo bleaching of methylene blue aqueous solution sensitized by composite powders of titanium oxide with SrTiO_3 , BaTiO_3 , and CaTiO_3 ," *Materials Transactions*, vol. 44, no. 10, pp. 2124–2129, 2003.
- [5]. T. Tsumura, K. Sogabe, and M. Toyoda, "Preparation of SrTiO_3 -supported TiO_2 photocatalyst," *Materials Science and Engineering B*, vol. 157, no. 1–3, pp. 113–115, 2009.

- [6]. H. Yang, C. Han, and X. Xue, "Photocatalytic activity of Fe doped CaTiO₃ under UV-visible light," Journal of Environmental Sciences, vol. 26, no. 7, pp. 1489–1495, 2014.
- [7]. H. Yoshida, L. Zhang, M. Sato et al., "Calcium titanate photocatalyst prepared by a flux method for reduction of carbon dioxide with water," Catalysis Today, vol. 251, pp. 132–139, 2015.
- [8]. A. Bhardwaj, N. V. Burbure, and G. S. Rohrer, "Enhanced photochemical reactivity at the ferroelectric phase transition in Ba_{1-x}Sr_xTiO₃," Journal of the American Ceramic Society, vol. 93, no. 12, pp. 4129–4134, 2010.
- [9]. Y. Miyasaka and S. Matsubara, in Proceedings of the 7th International Symposium on Application of Ferroelectrics (IEEE, Piscataway, NJ, 1991), p. 121 (1990).
- [10]. M. Viviani, M.T. Buscaglia, V. Buscaglia, L. Mitoseriu, A. Testino and P. Nanni, In Proceedings of the 13th IEEE International Symposium on Applications of Ferroelectrics, p. 103 (2002).
- [11]. Q. Yin, M. Ding, Y. Zhou, C. Tian, H. Lu and D. Zhao, Asian J. Chem., 24, 4095 (2012).
- [12]. K. K. Raina, P. Kumar and G. Sumana, Asian J. Chem., 18, 3384 (2006).
- [13]. V.N. Shut, S.R. Syrtsov and V.L. Trublovsky, Phys. Solid State, 53, 1859 (2011).
- [14]. X.H. Zhu, E. Defay, B. Guigues, G. Le Rhun, C. Dubarry and M. Aïd, J. Eur. Ceram. Soc., 30, 471 (2010).
- [15]. W. Zhang, Z. Xu, C. Wang and B. Zhao, Mater. Res. Bull., 38, 133(2003).
- [16]. K. Abe and S. Komatsu, J. Appl. Phys., 77, 6461 (1995).
- [17]. K.-T. Kim and C.-I. Kim, Microelectron. Eng., 66, 835 (2003).
- [18]. S.F. Liu, J.S. Liu, X.Z. Han and X.F. Zhang, Chem. Online, 67, w 30 (2004).
- [19]. J.S. Liu and G.N. Fan, Chin. J. Chem. Phys., 19, 367 (2006).
- [20]. Q. Jianquan, G. Zhilun, W. Yajing and L. Longtu, Mater. Chem. Phys., 73, 97 (2002).
- [21]. J. Zhang, J. Zhai and X. Yao, Scr. Mater., 61, 764 (2009).
- [22]. V.N. Shut, S.R. Syrtsov and V.L. Trublovsky, Phys. Solid State, 53, 1859 (2011).
- [23]. E. Avvakumov, M. Senna, N. Kosova, Soft Mechanochemical Synthesis, Kluwer Acad. Publ., Boston, 2002, p. 210.
- [24]. K. Wieczorek-Ciurowa, K. Gamrat, J. Therm. Anal. Calorim., 88, 213 (2007).
- [25]. Y. Tanaka, Q. Zhang, F. Saito, J. Mater. Sci., 39, 5497 (2004).
- [26]. N. Stevulova, T. Sverak, Chem. Listy, 99, 649 (2005).
- [27]. A. Gajovic, A. Santic, I. Djerdj, et al. Structure and electrical conductivity of porous zirconium titanate ceramics produced by mechanochemical treatment and sintering. J Alloys Compd, 479: 525-531, 2009.
- [28]. X. Ni, J. Ma, G. Li J, et al. Microwave characteristics of Co/TiO₂ nanocomposite prepared by mechanochemical synthesis. J Alloys Compd, 46: 386-39, 2009.
- [29]. X. Xu, JY Tang, T. Nishimura, et al. Synthesis of Ca-a-Si Al ON phosphors by a mechanochemical activation route. Acta Mater, 59: 1570-1576, 2011.
- [30]. T. Tojo, QW Zhang, F. Saito. Mechanochemical synthesis of FeSbO₄-based materials from FeO-OH and Sb₂O₅ powders. Powder Technol, 181: 281-284, 2008.
- [31]. Q. Hea, HZ Wang, GH Wen, et al. Formation and properties of Ba_xFe_{3-x}O₄ with spinel structure by mechanochemical reaction of Fe₂O₃ and BaCO₃. J Alloys Compd, 486: 246-249, 2009.
- [32]. T. Rojac, Ž. Trtnik, M. Kosec. Mechanochemical reactions in Na₂CO₃-M₂O₅ (M=V, Nb, Ta) powder mixtures: Influence of transition-metal oxide on reaction rate. Solid State Ion 1, 190: 1-7, 201.
- [33]. M. Golmohammad., Z.A. Nematì, M.A. faghihi sani Mater. Sci.-Poland, 28, 421, 2010.
- [34]. J. C. Tauc, Amorphous and Liquid Semiconductor. Plenum press, Newyork, 1974.
- [35]. H. Matsuda, M. Kuwabara, K. Yamada, H. Shimooka and S.Takahashi: J. Am. Ceram. Soc. 81, 3010, 1998.
- [36]. A.S. Chaves, R.S. Katiyar, S.P. Porto, S. Phys. Rev.B., 10, 3522, 1974.
- [37]. S. Tangwiwat, S.J. Milne, J. Non-Cryst. Solids, 351 (2005), 976.
- [38]. Miller F.A., Wilkins C.H., Anal. Chem., 24 (8) 1253, 1952.
- [39]. C.F. Kao, W.D. Yang., Appl. Organomet. Chem., 13, 383, 1999.

IOSR Journal of Applied Physics (IOSR-JAP) is UGC approved Journal with Sl. No. 5010, Journal no. 49054.

R.B.Ahirrao "Synthesis and Characterization of Nanocrystalline Barium Strontium Titanate Powder by Mechano-Chemical Method." IOSR Journal of Applied Physics (IOSR-JAP) , vol. 11, no. 2, 2019, pp. 45-51.